International Journal of Vehicle Design

ISSN online: 1741-5314 - ISSN print: 0143-3369
https://www.inderscience.com/ijvd

Design of BLDC motor drive system using alternative controllers for performance evaluation in electric vehicle applications

Mohanraj Nandakumar

DOI: 10.1504/IJVD.2024.10061812

Article History:

Received:	04 February 2021
Last revised:	06 August 2021
Accepted:	12 May 2022
Published online:	23 January 2024

Design of BLDC motor drive system using alternative controllers for performance evaluation in electric vehicle applications

Mohanraj Nandakumar

School of Electrical and Electronics Engineering,
SASTRA Deemed University,
Thirumalaisamudram, Thanjavur,
Tamil Nadu, 613401, India
Email: snehammohan@eee.sastra.edu

Abstract: Electric vehicles have emerged as a promising and alternative means of transportation, replacing IC engine driven automobiles. One important feature to be incorporated in an electric automobile is regenerative braking for extending the operating range. This paper discusses automobile dynamics, covering road friction, aerodynamic forces, transmission systems and calculation of tractive force. The time dependant profile of the reflected torque and speed variables at the motor shaft are computed and used as reference data for an intelligent controller. A multi-loop control scheme has been developed, with gain parameters tuned based on two alternate algorithms viz., particle swarm optimisation technique and multiple neuron fuzzy inference system for comparison. The experimental part is a representation of profile based operation, which deals with the application of the PMBLDC motor based drive system for powering a passenger car and the evaluation of the system performance. Power regeneration is validated and recorded.

Keywords: BLDC motor; electric vehicle; MNFIS; multiple neuron fuzzy inference system; PSO; particle swarm optimisation.

Reference to this paper should be made as follows: Nandakumar, M. (2024) 'Design of BLDC motor drive system using alternative controllers for performance evaluation in electric vehicle applications', *Int. J. Vehicle Design*, Vol. 94, Nos. 1/2, pp.57–82.

Biographical notes: Mohanraj Nandakumar working as Assistant Professor in SASTRA Deemed University. His areas of interests are power electronics drives and its controllers, control systems, microprocessors and microcontrollers and embedded systems.

1 Introduction

Alternate mode of transportation based on electric automobiles is globally gaining ground in recent years. Extensive research covering automobile design, associated electric motor drive systems and storage battery technology is being reported in the literature as significant areas for investigation. Although there is a major advantage in terms of reduced air pollution and noise, there is a major limitation of driving range, i.e., distance

per full charge of the main battery. The driving range can be increased by incorporating regenerative braking of the vehicle. During regeneration, the rectified back emf of the BLDC machine (Krishnan, 2001; Krause et al., 1995) charges the main/auxiliary battery, thereby recouping the kinetic energy of the automobile which also provides braking effect. Studies have shown that the use of regenerative braking can increase the driving range of an electric automobile (Ehsani et al., 2005) upto 15% under favourable conditions. However, regenerative braking has certain limitations in situations like low running speed in heavy traffic and the requirement of sudden stopping, which can be achieved only mechanically. Hence, a combination of regenerative braking followed by mechanical braking is required and is implemented by a single brake pedal seamlessly. BLDC motors are ideally suitable for electric automobiles because of their higher power to weight ratio, torque to current ratio, excellent torque-speed characteristics, high efficiency, wide range of speed, less maintenance and regeneration capability. Further, a BLDC motor drive system can operate over a wide range of speed, fed from a variable voltage and variable frequency inverter and drawing power from a battery. In practice, a controlled speed drive system requires a multi-loop controller consisting of an outer speed loop and an inner current loop for generating an actuating signal by implementing a control algorithm.

Recouping of kinetic energy in a battery-driven automobile while slowing down is attractive from the point of view of extending its range. A recent publication dealing with regeneration in an electric vehicle (Zhang et al., 2016) is focused on controlled charging of the battery using fuzzy sliding mode control technique. However, in this paper, variation of the state of charge (SOC) during the deceleration interval is not specifically reported. Moreover, an additional BLDC motor is coupled to the shaft of main motor, and speed control is done through a PID controller. An efficient regenerative braking system for electric/hybrid vehicles is reported in Naseri et al. (2016) where a front end DC-DC converter is introduced, which increases the hardware cost. This paper also presents ANN technique for speed control of the automobile. Another important publication (Torres-Sanz et al., 2018) deals with enhancing the efficiency of the charging process of batteries of electric vehicles at homes. Here, the focus is mainly on various alternate types of charging at of vehicles at residential areas but it does not cover SOC improvement by regenerative braking during travel. Various methods of regeneration are discussed in Godfrey and Sankaranarayanan (2018) where the main focus is towards choice of different methods and their comparisons. Further work for improving regenerative energy has been reported by Khanra et al. (2018) with focus on a conventional brushed DC motor based drive system and provided with a classic PI controller. According to Sain et al., permanent magnet synchronous motor (PMSM) (Sain et al., 2021) utilised in electric vehicles shows better dynamic response, improved torque-speed characteristics, reduced noise, energy-efficient operation, and less torque ripple. The highlights of this paper include the mathematical model of the PMSM drive system and use of particle swarm optimisation (PSO) technique for enhancing the drive performance. In the literature (Trimboli et al., 2022) main focus is on charging the battery packs utilised for electric vehicle i.e., on the regeneration interval but no emphasis is made on the acceleration and coasting interval. Pugi et al. (2021) discusses about super capacitor storage on electric buses and also about recharging. In Srivastava et al. (2021) different DC-DC converter topology used for recharging are compared during the

regenerative interval. Paper (Wang and Yang, 2021) presents the idea of wireless power transfer for charging electric vehicles through several compensation strategies. A control strategy using Genetic algorithm (Li et al., 2021) electric vehicle is discussed for charging. Liu et al. (2020) suggested fuzzy method for charging electric vehicle during regenerative period. Chen et al. (2020) proposed an idea of tuning of PI parameters using fuzzy for control of PMSM used in electric vehicles. Induction motor (Elnaghi et al., 2020) utilised to drive electric vehicle and motor operation is controlled by inverter suggested by Basem E. Elnaghi et al. during regenerative period (Wu et al., 2020), an optimal regenerative braking torque of permanent-magnet synchronous motor in electric vehicles is discussed. Li et al. (2020) suggested a method of fault diagnosis for electrified vehicles for model based techniques. Modelling of hybrid fuel cell (Srikanth and Venkatesan, 2020) and design of solar based for electric vehicle proposed by Tianpei Li et al. A new hybrid salp swarm algorithm and radial basis function-based approach for electric vehicle and a robust design for it were proposed by Yıldız (2020). An overview of electric vehicle converter configurations, control methods and charging techniques for the three regions speed-time curve elaborated by Indragandhi et al. (2020), and research was provided by Proff et al. (2019), for storing the regenerative energy in battery and transfer it to the grid. A newly developed hybrid converter for electric vehicle battery charging with power quality features is dealt by Ananthapadmanabha et al. (2019). Several authors (Divakarla et al., 2019) developed an algorithm using artificial neural network based adaptive control for plug-in hybrid electric vehicles.

The major focus of the work now being reported is to examine the suitability and evaluation of performance of a PMBLDC motor drive system while driving an electric vehicle. Accordingly, the problem formulation incorporates the total model of electric vehicle, BLDC motor based drive system, rechargeable battery, power electronic modulators and controllers governed by two alternative control algorithms viz., PSO and MNFIS. The investigation first creates speed and torque profiles to serve as reference characteristics to the controller for effective closed loop operation of the drive. The first part of the paper deals with the initial acceleration and coasting intervals, corresponding to motoring mode in Quadrant I. Energy recouping is considered in the second part when the BLDC machine runs as a generator in Quadrant II. Here, comparison of two alternate power circuit configurations is carried out to identify the better of the two schemes.

The organisation of paper is as follows. Section 2 presents the block diagram of Automobile and Drive System along with a brief description. In Section 3 fundamental equations governing an automobile, leading to its dynamic model are discussed. Equations related to modelling of BLDC Motor are presented in Section 4. Section 5 introduces and explains two different control algorithms for closed loop operation of the drive. In Section 6, methods of regeneration are dealt with. In Section 7 simulation schematics for modelling the automobile and drive system are created. Simulation results are discussed in Section 8. The experimental set up is discussed in Section 9. Finally, in Section 10 the concluding statements emphasis on comparing the results obtained in both controllers and among them which provides better results are stated.

2 Block diagram of automobile and drive system

The essential functional blocks present in the electric vehicle are shown in Figure 1. One major block is the mechanical/mathematical automobile model based on dynamic equations related to road friction at the wheels, wind forces and viscous friction of power transmission including gear box. The second part includes the modelling of the electrical system containing main battery, 6-pulse inverter (Moorthi, 2005; Rashid, 2011), 4-pole BLDC motor along with controller and control loops. The controller configuration is made up of an outer speed loop and inner current loop with respective error signals to produce a reference current variable so as to develop the required shaft torque. The control action is realised through two alternate control algorithms, viz., PSO or multiple neuron fuzzy inference system (MNFIS).

Figure 1 Automobile model and BLDC motor drive system (see online version for colours)

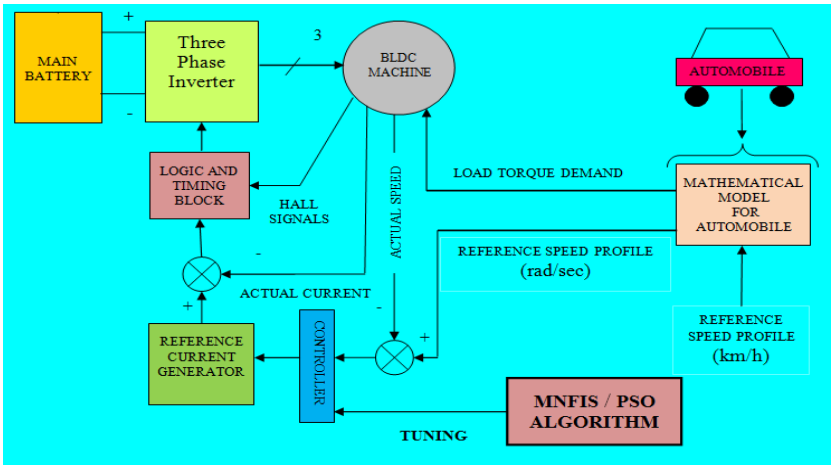

3 Dynamic modelling of automobile

Development of a dynamic model of an automobile during forward run has to consider various aspects like road friction at the tyres to be overcome, frictional forces related to the transmission system and the aerodynamic resistance due to relative velocity in air (Ehsani et al., 2005). These are discussed below

(a) *Force due to wind resistance* (F_w)

It is drag resistance due to wind as the vehicle drives forward and is given below

$$F_w = 0.5\,\rho\,A\,v^2 C_w \tag{1}$$

where F_w is wind force, ρ is Air density, A is vehicle frontal area, v is Driving velocity, all in SI units, C_w is Drag coefficient.

(b) *Force due to rolling resistance* (F_R)

This resistance is due to the friction between wheels and road. It is calculated as

$$F_R = m\,g\,f_r \tag{2}$$

m is mass of the vehicle, kg, g is acceleration due to gravity, m/s^2 and f_r is rolling friction coefficient

(c) *Force due to mechanical and bearing friction* (F_B)

The rotating mechanical parts such as bearing, shaft and others offer some resistance. This resistance not only depends on their installation with proper alignment during manufacturing but also on lubrication (Ehsani et al., 2005).

$$F_B = m\,g\,f_b \tag{3}$$

where f_b is bearing friction coefficient

The total force F_s required for the forward motion of the automobile is the sum of the above components and is expressed as below in Newton.

$$F_s = F_w + F_R + F_B \tag{4}$$

The next steps to be calculated are the driving axle (shaft) speed and shaft torque as given below

(d) *Shaft speed* (N_s)

Shaft speed is obtained by dividing by the linear velocity of the vehicle and the circumference of the driving wheel is expressed as

$$N_s = \frac{60 * v}{\Pi * D_{wheel}} \text{ RPM} \tag{5}$$

where $D_{wheel} = D_{rim} + 2H$

D_{wheel} is wheel diameter, D_{rim} is Rim diameter and H is radial thickness of the tyre, all in m.

(e) *Shaft torque* (T_s)

Shaft torque is the product of the shaft force and wheel radius

$$T_s = F_s * R_{wheel} \tag{6}$$

where R_{wheel} is wheel radius

The BLDC motor shaft torque T_m and speed n_m are obtained by the following relations

(f) Motor torque (T_m)

$$T_m = \frac{T_s}{k * \acute{\eta}} \tag{7}$$

where $\acute{\eta}$ is gearbox efficiency, k is gear ratio

(g) *Motor speed* (n_m)

$$n_m = N_s * k \tag{8}$$

Starting with a speed-time curve shown in Figure 2, so as to reflect the initial acceleration and forward run corresponding to typical road conditions, the required speed time profile

at the motor shaft is computed. Further, using equations (1)–(8) describing the mechanical and aero-dynamic characteristics, the corresponding torque demand profile at the BLDC motor shaft over the total interval is obtained through SIMULINK (MathWorks, 2016) schematic.

Figure 2 Speed-time profile of automobile (see online version for colours)

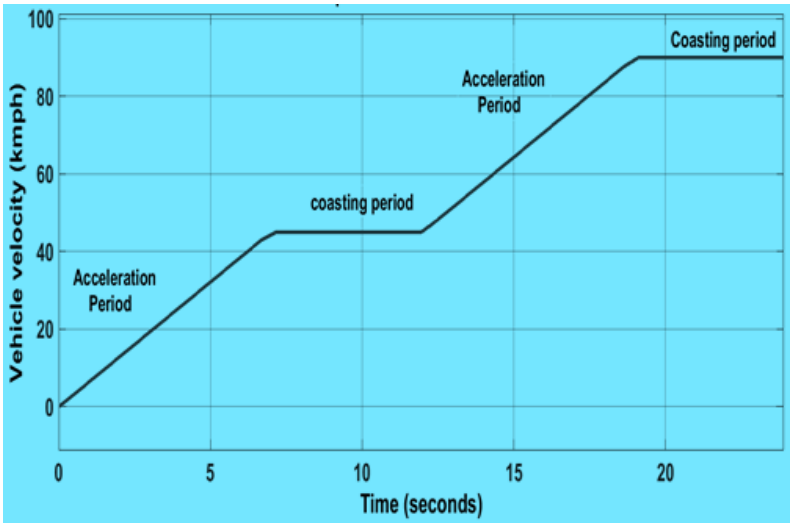

4 Modelling of BLDC motor

The stator voltage and current relationship in a BLDC motor is described by the following vector-matrix equation

$$\begin{bmatrix} V_{Rn} \\ V_{Yn} \\ V_{Bn} \end{bmatrix} = \begin{bmatrix} R & 0 & 0 \\ 0 & R & 0 \\ 0 & 0 & R \end{bmatrix} \begin{bmatrix} i_R \\ i_Y \\ i_B \end{bmatrix} + \begin{bmatrix} L-M & 0 & 0 \\ 0 & L-M & 0 \\ 0 & 0 & L-M \end{bmatrix} \frac{d}{dt} \begin{bmatrix} i_R \\ i_Y \\ i_B \end{bmatrix} + \begin{bmatrix} e_R \\ e_Y \\ e_B \end{bmatrix} \tag{9}$$

In the above, balanced stator voltages ($V_{Rn}\, V_{Yn}\, V_{Bn}$) and currents ($i_R\, i_Y\, i_B$), ($e_a\, e_b\, e_c$) are the back EMF in the respective phase windings, equal values of stator winding resistances (R), self-inductance (L) and mutual inductances (M) along with 120° conduction mode of the inverter are assumed.

The electromagnetic torque T_e developed by the motor is given by

$$T_e = \frac{e_R i_R + e_Y i_Y + e_B i_B}{\omega} \tag{10}$$

Equating the developed torque $T_e(t)$) with the mechanical torque demand $T_m(t)$ and invoking the torque-balance equation (11) given below enables evaluation of the actual speed $\omega(t)$ of the motor.

$$T_e(t) = J \frac{d\omega_m(t)}{dt} + B\ \omega_m(t) + T_L(t) \tag{11}$$

where J = equivalent rotational moment of inertia of the automobile mass, B = equivalent viscous and wind friction coefficient and, T_L = equivalent load torque, all referred to the motor shaft.

5 Control algorithms

The BLDC motor drive system is required to follow a specific speed-time characteristic of the automobile in tune with a profile, as decided by driver preferences and traffic conditions. The control action begins by sensing the instantaneous speed error, which is processed by a control algorithm to generate a current reference, sent to a hysteresis controller to create gate trigger signals for six IGBT switches of the inverter. In this paper two powerful control algorithms viz., PSO and MNFIS are made use of and are discussed below.

5.1 Particle swarm optimisation

Particle swarm optimisation (PSO) algorithm is a population based soft computing technique inspired by social behaviour exhibited by a flock of birds or school of fish. It tries to mimic the group communication philosophy of sharing individual experience in achieving an optimal solution for locating food. In this method, a population swarm is initialised with random positions S_i and velocities V_i. At the beginning, the population is scattered randomly throughout the search space and the flying individuals successively adjust their direction and velocities for optimisation of the performance criterion, based to their own experience and the experience of their companions.

In PSO, Moussouni et al. (2008) each element is a 'bird' in the search space; this is referred to as a "particle". The swarm is modelled as particles in a three-dimensional space, which have their own positions and velocities. These particles have two essential abilities: memory of their own best position and knowledge of the global best as a consequence of intercommunication. The best position achieved so far by a particle is denoted as $P_{best}(P_i^t)$ and the globally best position achieved by any particle in the population is denoted as $G_{best}(G_i^t)$.

The updated velocity of each particle is calculated using the present velocity and the distances from P_{best} and G_{best} and is expressed in the following equations:

$$V_i^{t+1} = W \cdot V_i^t + C_1 \cdot R_1 \cdot \left(P_i^t - S_i^t\right) + C_2 \cdot R_2 \cdot \left(G_i^t - S_i^t\right) \tag{12}$$

where V_i^t and S_i^t are the velocity and position of ith particle, C_1 and C_2 are cognitive parameter and social parameter, R_1 and R_2 are the random variables in the range [0,1].

$$S_i^{t+1} = S_i^t + V_i^{t+1} \tag{13}$$

The updated velocity and the position are given in equations (12) and (13), respectively.

The inertia weight (W) will decrease linearly during optimisation run and is given by the formula

$$W = W_{max} - \left(\frac{W_{max} - W_{min}}{Iteration_{max}} \right) \times Ct_{Iter} \tag{14}$$

where W_{max} and W_{min} are the maximum and minimum value of inertia weight, Ct_{Iter} is the current iteration and $Iteration_{max}$ is the maximum number of iterations.

Equation (14) shows the inertia weight. The PSO algorithm is incorporated as a m-file linked with SIMULINK for dynamic tuning of controller parameters and its flowchart is shown in Figure 3.

Figure 3 Flowchart of PSO

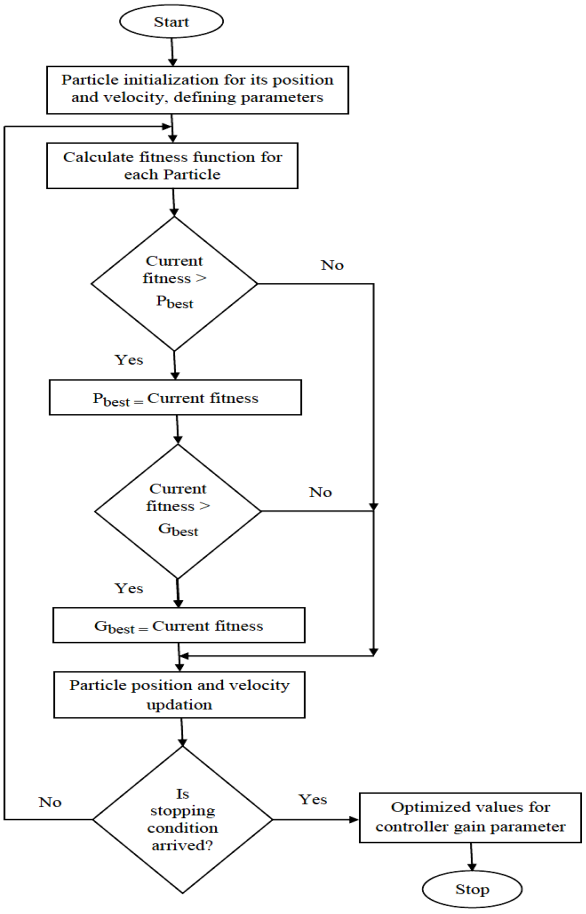

5.2 *Multiple neuron fuzzy inference system (MNFIS) model*

The MNFIS model as proposed by Tagaki-Sugeno (Wu et al., 2020) is shown in Figure 4, which, in general, can consist of several layers and interconnected nodes. Here, there are two inputs and one output with three intermediate layers. If-then rules form a rule base and their relationship is governed by a set of equations as given below:

If a_1 is P_1 and a_2 is Q_1 then $b_1 = r_{11}\, a_1 + r_{12} a_2 + r_{10}$ and (15)

If a_1 is P_2 and a_2 is Q_2 then $b_2 = r_{21}\, a_1 + r_{22} a_2 + r_{20}$, then (16)

$$b = \frac{w_1 b_1 + w_2 b_2}{w_1 + w_2} = \overline{W}_1 b_1 + \overline{W}_2 b_2 \tag{15}$$

where w_1, w_2, $\overline{W}_1, \overline{W}_2$ are updated weights in the respective layers.

Figure 4 Structure of multiple neuron fuzzy inference system (MNFIS) (see online version for colours)

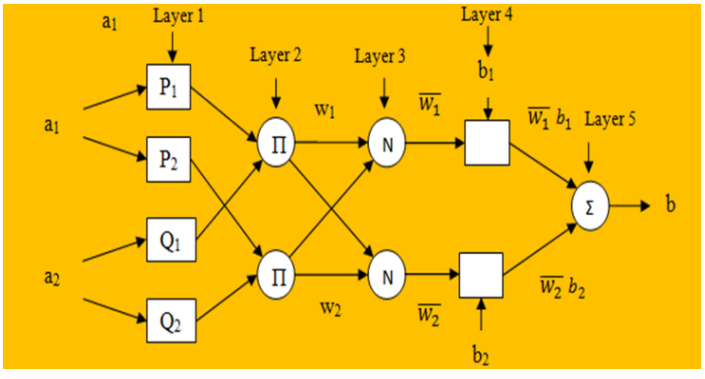

Layer 1

Each node considered in this layer is an adaptive node and is represented by j and the function of each node is given by

$$F_{1,j} = P_j(a_1) \text{ for } j = 1, 2 \tag{16}$$

$$F_{1,j} = Q_{j-2}(a_2) \text{ for } j = 3, 4 \tag{17}$$

Layer 2

In this layer, each node is called a fixed node and is labelled as Π. The output from this node is the product of all incoming signals.

$$F_{2,j} = w_j = P_j(a_1)\, Q_j(a_2) \text{ for } j = 1, 2 \tag{18}$$

Layer 3

In this layer, each node is called fixed node and is labelled as N. Here, jth node determines the ratio between strength at that instant of firing to the sum of all strengths.

$$F_{3,j} = \overline{w}_j = \frac{w_j}{w_1 + w_2} \text{ for } j = 1,2 \tag{19}$$

Layer 4

In this layer, each node is called adaptive node and is represented by the function

$$F_{4,j} = \overline{w}_j\, b_j = \overline{w}_j\, (r_{j1}\, a_1 + r_{j2} a_2 + r_{j0}) \tag{20}$$

for $j = 1, 2$ and where the normalised transmission $\bar{w}_j$ is obtained from previous layer and $\{rj1, rj2, rj0\}$ are called consequent parameters.

Layer 5

This is called as an output layer and is represented by Σ, which computes the overall output.

$$F_{5,j} = \sum_j \bar{w}_j bj = \frac{\sum_j w_j bj}{\sum_j w_j} \text{ for } j = 1, 2 \tag{21}$$

In this paper, the MNFIS algorithm captures the two signals viz., the error (e) between reference and actual speed of the BLDC motor and also its derivative (de), which generate a set of transmission parameters. These parameters are successively updated for convergence so as to generate Fuzzy Inference System consisting of fuzzified variables, their membership functions and the defuzzified output. The resulting fuzzy based rule table is given below in Table 1.

Table 1 Rule base framed for fuzzy logic inference system

de \ *e*	*NV*	*NB*	*NM*	*NS*	*ZE*	*PS*	*PM*	*PB*	*PV*
NV	NV	NV	NV	NV	NV	NB	NM	NS	ZE
NB	NV	NV	NV	NV	NB	NM	NS	ZE	PM
NM	NV	NV	NV	NB	NM	NS	ZE	PM	PM
NS	NV	NV	NB	NM	NS	ZE	PS	PM	PB
ZE	NV	NB	NM	NS	ZE	PS	PM	PB	PV
PS	NB	NM	NS	ZE	PS	PM	PB	PV	PV
PM	NM	NS	ZE	PS	PM	PB	PV	PV	PV
PB	NS	ZE	PS	PM	PB	PV	PV	PV	PV
PV	ZE	PS	PM	PB	PV	PV	PV	PV	PV

Where NV is Negative Very Big, NB is Negative Big, NM is Negative medium, NS is negative Small, ZE is Zero, PV is Positive Very Big, PB is Positive Big, PM is Positive medium, and PS is Positive small.

The final actuating signal obtained after defuzzification is the torque reference variable using which three reference phase currents are determined.

6 Alternate methods of regeneration

The motoring operation of the drive system covers the period of an initial acceleration till the end of coasting. The braking phase of the vehicle can be advantageously used for recouping a major part of the kinetic energy. In this paper, two regeneration schemes viz.,

i one-switch regeneration (Nian et al., 2014)

ii auxiliary battery regeneration (Moussouni et al., 2008) are introduced and are described below.

6.1 One-switch regeneration

Figure 5 shows the regeneration circuit of one-switch conduction method where no new hardware is required, but the power circuit is operated in converter mode of operation of inverter, enabling reverse power flow from the BLDC machine to the main battery. The principle of a boost DC-DC converter is employed as shown in Figure 8. Here, all the IGBT switches of the inverter except the lower switch of phase A arm are kept open. The lower IGBT of A phase is switched in a PWM manner for boosting the reverse DC voltage by utilising the leakage inductance L of phase A and the DC link capacitor. This circuit is analysed and the maximum conversion ratio is derived as follows:

Figure 5 Equivalent circuit of 1-switch regeneration (see online version for colours)

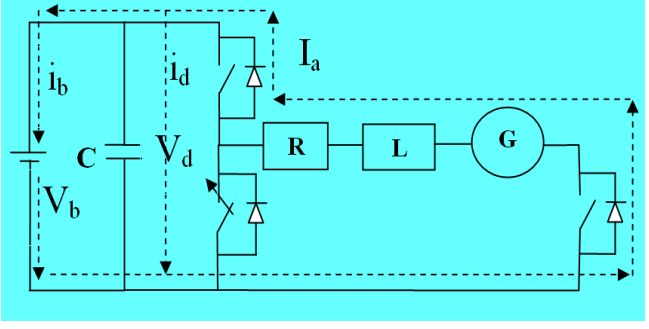

Figure 6 Auxiliary battery connection to BLDC machine (see online version for colours)

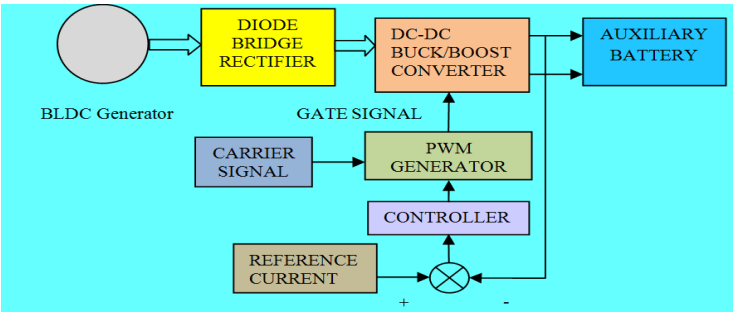

According to the principle of the volt-second balance (Krause et al., 1995), one can conclude that the net change in the equivalent inductor voltage v_L is zero over one electric cycle, i.e.,

$$\int_{t}^{t+T_s} V_L \mathrm{d}t = DT_s\,[2V_e - i_a(2R)] + D'\,T_s\,[2V_e - i_a(2R) - V_d] = 0 \tag{22}$$

where T_s is switching period , V_e is back EMF, i_a is stator current, R is internal resistance, R_b is equivalent load resistance, V_d is charging voltage and D is duty ratio which satisfies $D + D' = 1$

Figure 7 Complete model of automobile integrated with drive system in MATLAB/SIMULINK

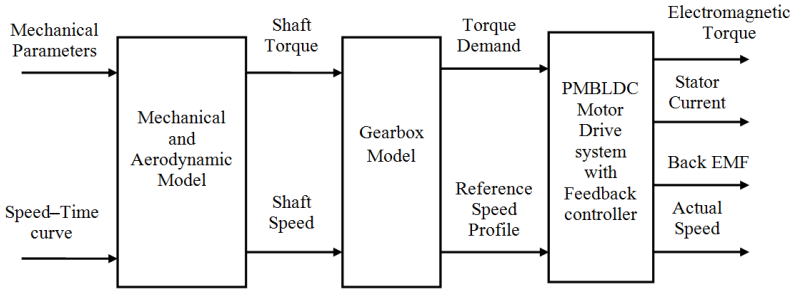

Figure 8 Model of automobile in MATLAB/SIMULINK

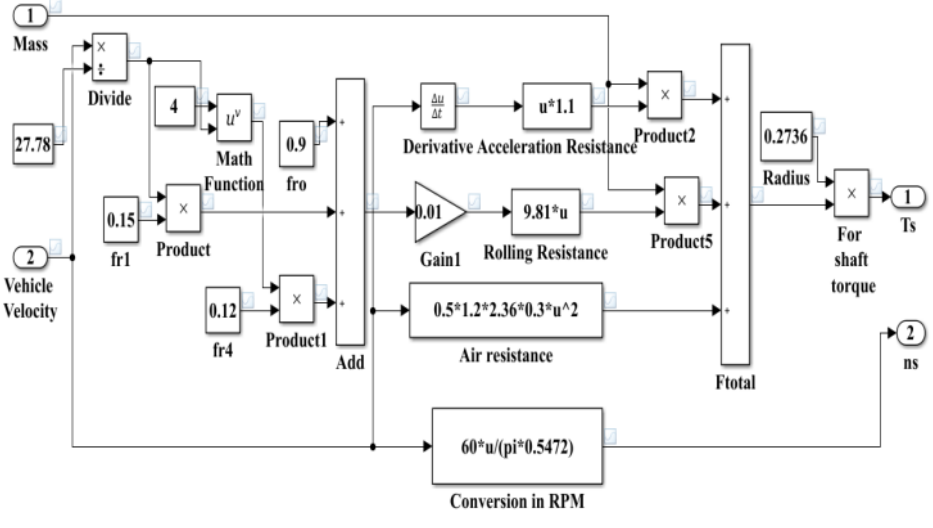

After simplification we get

$$i_a = \frac{2V_e - D'V_d}{2R} \tag{23}$$

where V_e is the instantaneous phase voltage, V_d is the DC link voltage, D is the duty ratio and R the resistance of one phase of motor winding.

According to the principle of the capacitor charge balance,

$$\int_t^{t+T_s} i_{dc}\,\mathrm{d}t = DT_s\left(-\frac{V_d}{R_b}\right) + D'\ T_s\left(i_a - \frac{V_d}{R_b}\right) = 0 \tag{24}$$

The conversion ratio γ (D') is obtained from equations (23) and (24)

$$\gamma\ (D') = \frac{V_d}{V_e} = 2\left(\frac{1}{D' + 2\left(\frac{k}{D'}\right)}\right) \text{ Where } k = \frac{R}{R_b} \tag{25}$$

where R_b is the internal resistance of main battery circuit

To evaluate the maximum conversion ratio of the witching

$$\frac{d\gamma}{dD'} = 2\frac{\left(2k - D'^2\right)}{\left(D'^2 + 2k\right)^2} \tag{26}$$

and the value of D' which maximises γ as

$$\gamma_{max}(D')|_{D'=\sqrt{2k}} = \frac{1}{\sqrt{2k}} \tag{27}$$

The above method of regeneration is implemented by controlling the lower switch of phase A using a PWM signal with duty ratio $D = 1 - \sqrt{2k}$ for maximising energy recapture.

Figure 9 BLDC motor drive model in MATLAB/SIMULINK (see online version for colours)

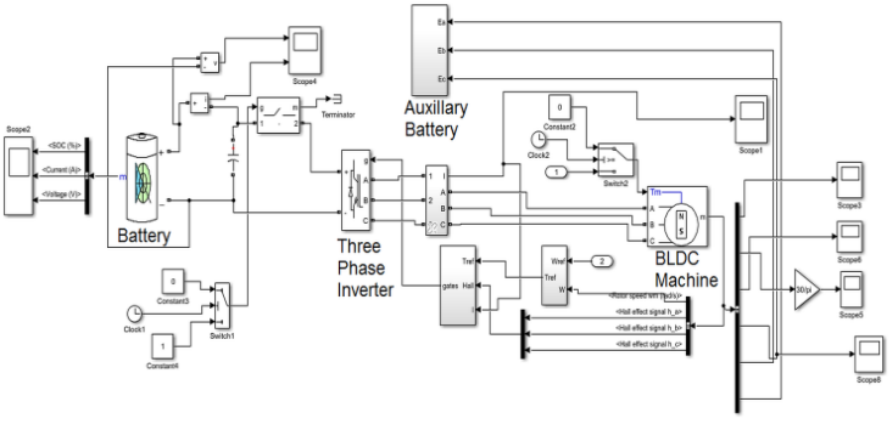

6.2 Auxiliary battery regeneration

Regeneration circuit using an auxiliary battery connected to the BLDC machine through a three phase diode bridge rectifier and a controlled DC-DC buck/boost converter is shown in Figure 9. As and when the traffic condition requires slowing down of the vehicle, the driver releases the acceleration pedal and operates the brake pedal of which the initial movement cuts off the power from the main battery and simultaneously connects the auxiliary battery through a changeover switch. It is advisable to charge the auxiliary battery with constant current charging during the regeneration interval for longer battery life. Hence a dedicated feedback current controller using duty ratio control of the DC-DC buck/boost converter is implemented. Here also the controller is designed based on two

alternate algorithms viz., PSO/MNFIS as shown in Figure 6. For facilitating energy recouping in the auxiliary battery, it is necessary to maintain its SOC has to be maintained at around 50%, which is adequate for energising selected auxiliary loads in the automobile like wind screen wiper, power window, dashboard lighting etc.

7 Simulation schematics

The simulation schematic shown in Figure 7 consist two major subsystems – the automobile model and the BLDC motor based electrical drive subsystem, which includes the main battery, feedback loops and also one of the two alternate modules holding the PSO and MNFIS algorithms. The automobile subsystem translates the fundamental equations (1)–(8) describing the forces corresponding to rolling friction at the wheels, mechanical and bearing friction and aerodynamic resistance and computes the equivalent torque demand at the motor shaft. The controller of the BLDC motor drive system schematic receives the set speed as a reference input along with actual speed and initiates control action as described in Section 5. The technical specifications of Nissan considered for modelling is shown in Table 2.

Table 2 Technical specifications of Nissan Leaf model

Parameter	*Value*	*Unit*
Vehicle mass	1521	Kg
Vehicle frontal area	2.21	m^2
Drag coefficient	0.29	
Tyre friction coefficient	0.01	
Wheel diameter	0.6468	m
Gear ratio	4.2	
Gear efficiency	0.92	

7.1 Modelling of automobile

The subsystem calculates forces corresponding to rolling friction at the wheels, aerodynamic resistance and mechanical and bearing friction and computes the equivalent torque at the driving shaft shown in Figure 8.

7.2 Modelling of the drive system

Figure 9 shows the SIMULINK schematic of BLDC motor drive system where the automobile drive requirements are represented by the speed profiles as discussed in Section 3 and shown in Figure 3 and is a subsystem in the overall schematic diagram in Figure 9. Figure 12 also contains a DC link energised from main battery supplying power to the 6-pulse inverter and the BLDC motor for initial start, acceleration and coasting of the automobile After reaching a steady speed, as and when rapid braking is required, the same is achieved by regeneration (Sain et al., 2021) into an auxiliary battery, which is rated at a lower voltage. The detailed schematic of this regeneration circuit is shown in

Figure 10, where the back EMF is rectified to feed a DC-DC boost converter to operate in current controlled mode to ensure safe and efficient charging of the auxiliary battery.

Figure 10 Auxiliary battery connection model in MATLAB/SIMULINK (see online version for colours)

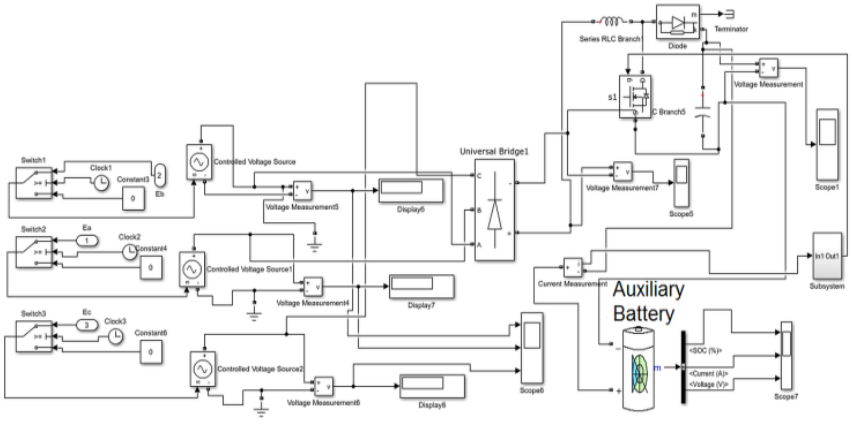

The schematic represents an alternate means of regeneration, which employs a one switch PWM control on phase A lower switch of the 6-pulse inverter, where converter operation of the inverter is realised along with a voltage boost action in the reverse direction, resulting in regenerative braking operation is shown in Figure 11.

Figure 11 One switch conduction model in MATLAB/SIMULINK (see online version for colours)

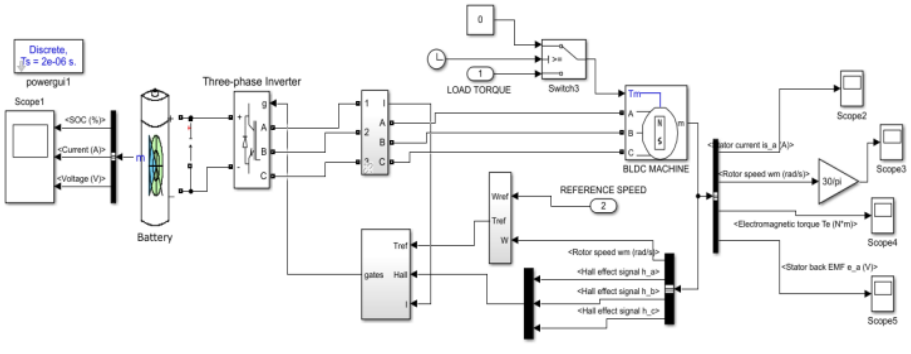

7.3 Regeneration modes

For implementing regeneration mode, two alternate schemes viz., auxiliary battery and one switch conduction methods have been incorporated and are shown in Figures 10 and 11. Both the schemes are utilised for regeneration using

i PSO

ii MNFIS based control techniques.

8 Simulation results

8.1 Acceleration and coasting period

Figures 7–11 covering automobile dynamics, BLDC motor drive system model and two alternate controllers are simulated for an interval of 18 s covering the three modes of operation of the automobile, viz., acceleration, coasting and regeneration. The simulation results of the drive, in terms of motor speed, torque and stator back emf are obtained. The time interval of 0–17 s in Figure 12(a) and (b) depict the variation of motor speed with time during the acceleration and coasting period for the PSO and MNFIS controllers respectively. This indicates the degree of effectiveness of the overall control scheme discussed in Section 5. Figure 13(a) and (b) portray the variation of back emf of phase A as the vehicle picks up speed and attaining a steady speed when employing the 2 controllers. The actual trapezoidal waveform of the stator emf is verified by expanding a small portion of the same. The rapid development of shaft torque through control of stator current is a crucial aspect of the performance of the automobile and this is clearly exhibited in Figures 14(a), (b) and 15(a), (b) as important simulation results. The initial large current and torque during acceleration, followed by their gradual reduction subsequently is typical in an electric vehicle. The stator current waveform in the expanded view is consistent with the 120° conduction mode of the inverter. Regarding the behaviour of the main battery, it is maintaining the voltage, but the SOC gets diminished during the interval 0–17 s and the recharging due to the one-switch conduction method is very limited. The control algorithms are compared based on various time domain specifications and well-defined integral error indices are tabulated in Table 3.

Figure 12 Shaft speed variation with time: (a) PSO and (b) MNFIS (see online version for colours)

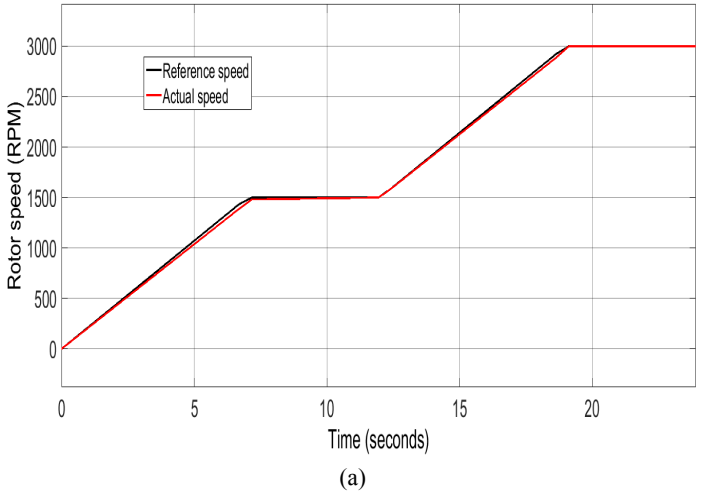

(a)

Figure 12 Shaft speed variation with time: (a) PSO and (b) MNFIS (see online version for colours) (continued)

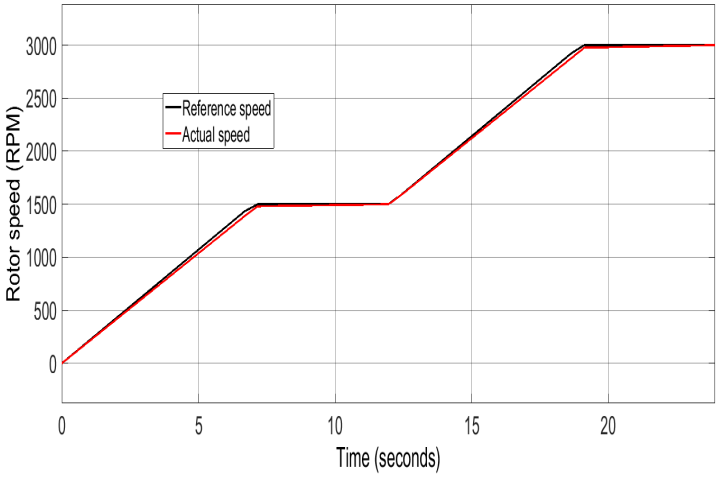

(b)

Figure 13 Back emf waveform variation with time: (a) PSO and (b) MNFIS (see online version for colours)

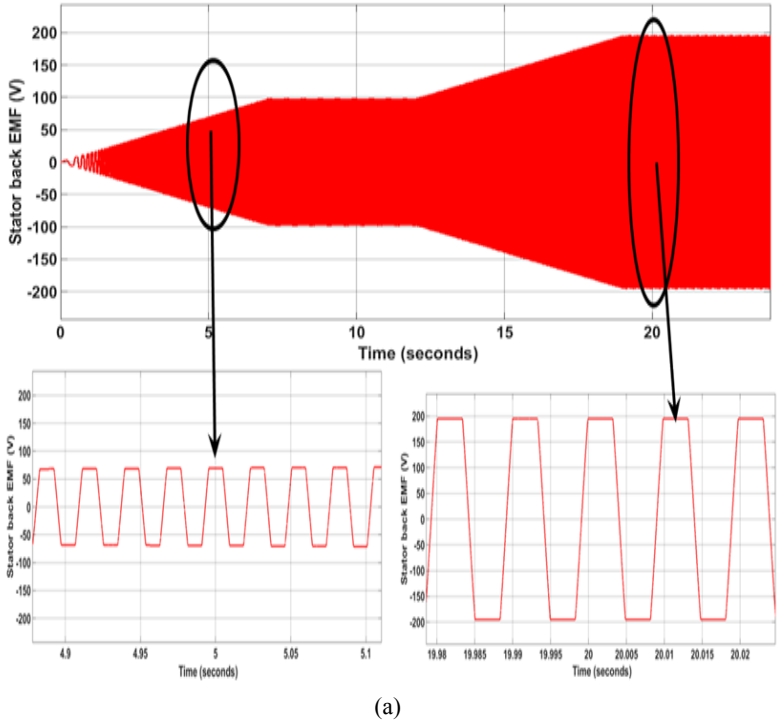

(a)

Figure 13 Back emf waveform variation with time: (a) PSO and (b) MNFIS (see online version for colours) (continued)

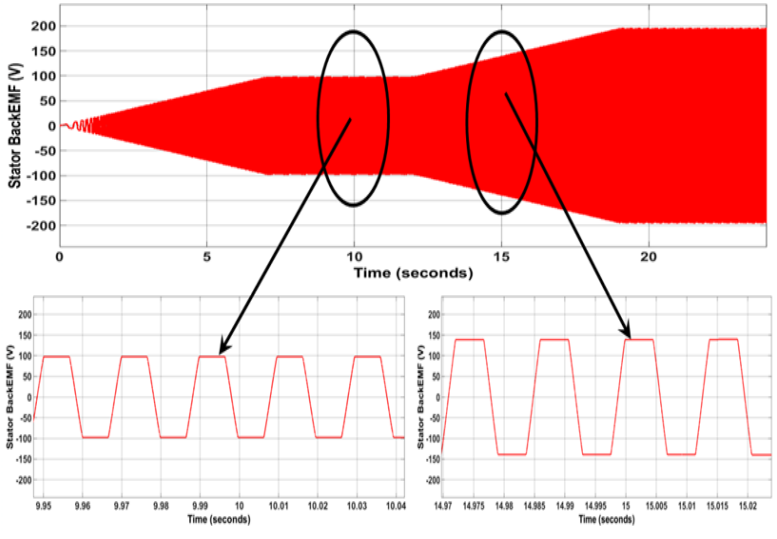

(b)

Figure 14 Electromagnetic torque variation with time: (a) PSO and (b) MNFIS (see online version for colours)

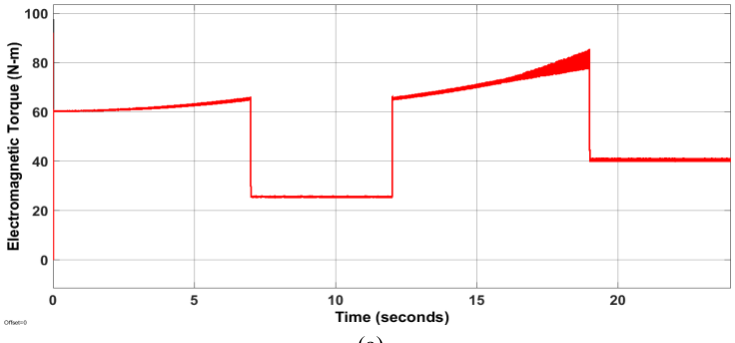

(a)

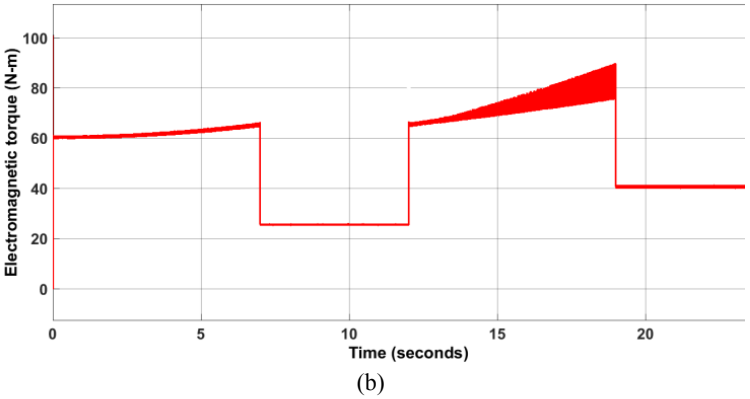

(b)

Figure 15 Stator current variation with time: (a) PSO and (b) MNFIS (see online version for colours)

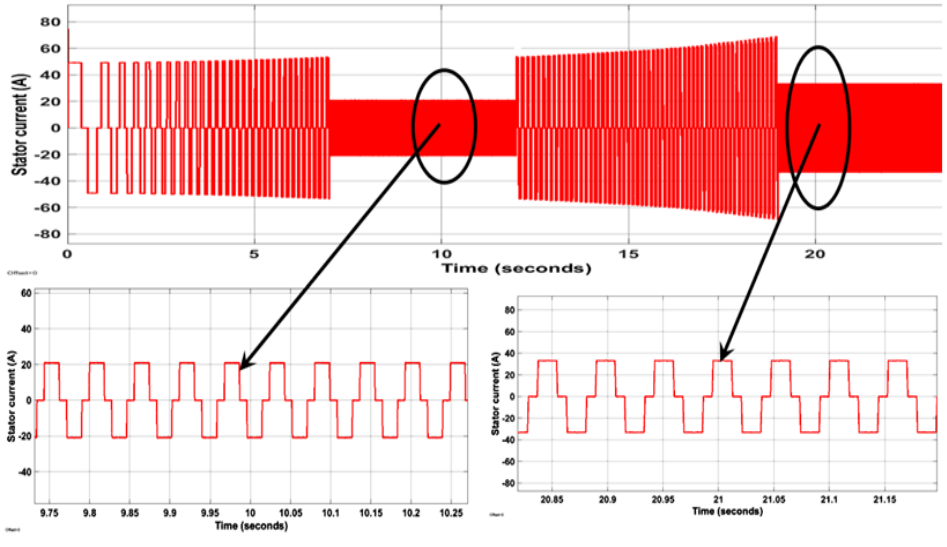

(a)

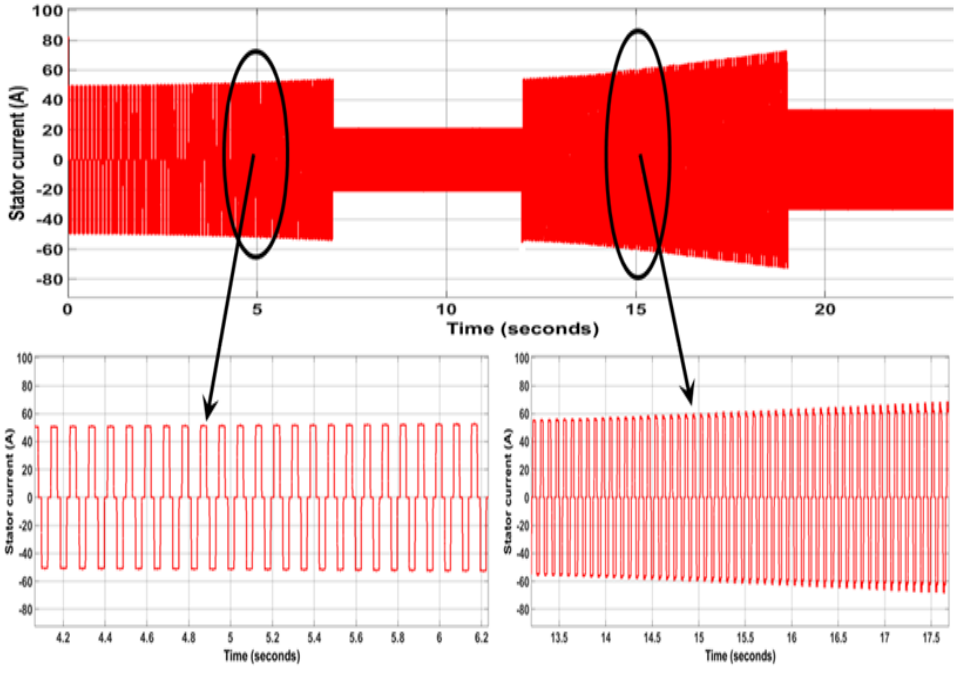

(b)

Table 3 Comparison of control algorithms and integral criteria

Parameters	*MNFIS*	*PSO*
Rise time (sec)	0.0672	0.0372
Settling time (sec)	0.0760	0.0460
Peak overshoot (%)	0.5079	3.2519e-4
Steady state error	0.0461	0.0023
Integral square error (ISE)	$1.007e^{+4}$	$1.007e^{+4}$
Integral absolute error (IAE)	$9.395e^{+6}$	$9.387e^{+6}$
Integral time absolute error (ITAE)	$1.464e^{+5}$	$1.459e^{+5}$

8.2 Regeneration interval

The regeneration interval starts at 17 s, when the automobile is required to slow down. The simulation results corresponding to the same are also shown in Figures 12–15 covering variation of speed, stator current, back emf and torque. Figure 16 depicts the variation of SOC of the main battery covering the full interval indicating the discharge during the initial periods (0–18 s) and regeneration subsequently. As far as the auxiliary battery is concerned, the SOC remains unchanged during the interval 0–17 s and shows a significant rising behaviour thereafter as shown in Figure 17.

Figure 16 State of charge (SOC), voltage and current waveforms of main battery (see online version for colours)

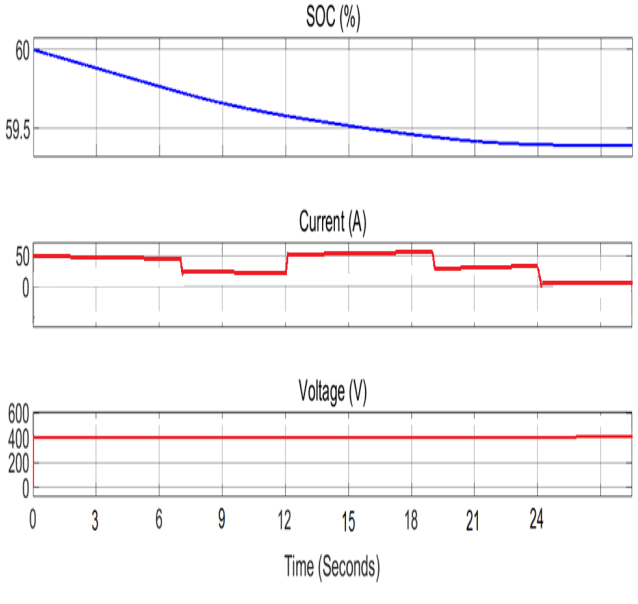

Figure 17 State of charge (SOC), voltage and current waveforms of auxiliary battery (see online version for colours)

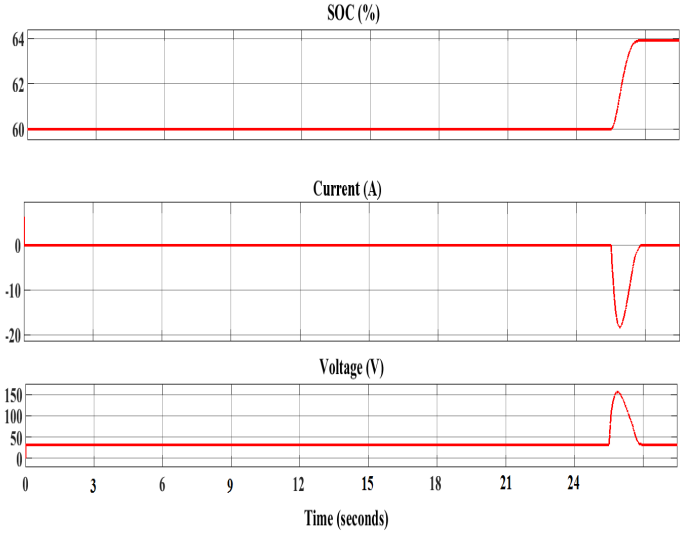

9 Experimental work

The experimental set up consists of BLDC motor coupled to a DC generator with a load resistive bank, Intelligent Power Module and facility for speed measurement. The control hardware incorporates an ARM CORTEX M4F microcontroller in a development board. It is also provided with desktop PC interfaced with the development board and SIMULINK based graphical user interface (GUI) is created for display of reference speed actual speeds of the motor in the PC terminal. Figure 18 shows a snapshot of the experimental set up and related instrumentation. The control module for the above system is created containing various communication interface blocks supported with a PSO control algorithm along with input and output signal definitions. This model is used for building a source file and compiling it together with.asm and .hex files. This .hex file is then downloaded to the flash memory of the ARM microcontroller board, which is interfaced with the Intelligent Power Module for gate triggering of six IGBT switches.

Figure 18 Experimental set up and its related instrumentation (see online version for colours)

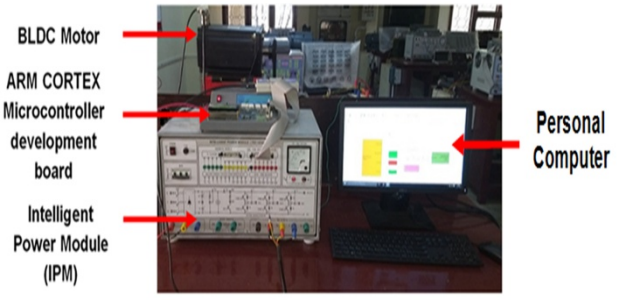

9.1 Acceleration and coasting

The drive system is operated from a 3-phase 200 V mains supply through a diode bridge rectifier and a 6-pulse inverter. The feedback variable corresponding to speed is first signal conditioned and interfaced with the ARM cortex board using the inbuilt ADC for closed loop operation. Here the reference speed profile is a representive speed-time curve which reflects the traffic/road conditions and driver response over the acceleration and coasting interval. Figure 19 shows this reference speed profile and actual motor speed, which are captured as a display on the online monitor over a period of 10 s. It is seen that the actual speed follows the reference setting with a certain time lag.

Figure 19 Real time GUI monitoring with increasing values of the actual and set speed of BLDC motor (see online version for colours)

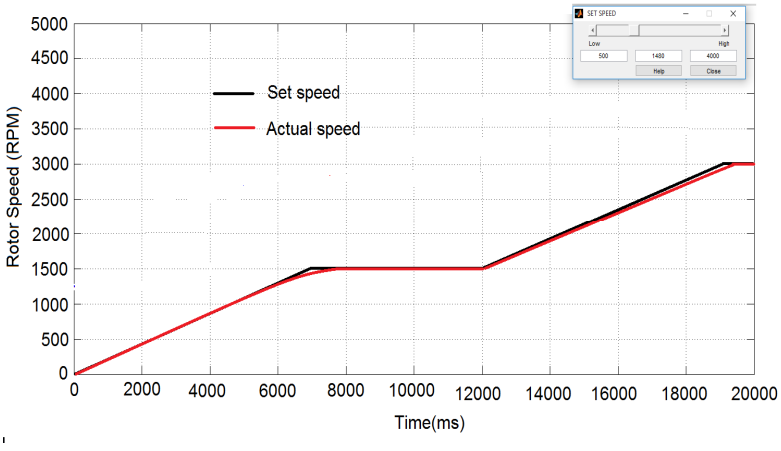

9.2 Regeneration

For experimental validation of the regeneration phase of the operation, the drive system is first run corresponding to the coasting stage at a speed of 1500 rpm. The recapture of the stored energy is facilitated by turning off the gate triggering of all 6 IGBT's, thereby enabling the converter operation of the 6-pulse inverter though the anti-parallel diodes. Simultaneously the mains supply to the DC link capacitor is disconnected to enable additional charging of the same by reverse power flow. The experimental work captures in a digital storage oscilloscope (DSO) the step increase of the capacitor voltage due to the back feeding of the rectified BLDC generator output and its subsequent discharge through a resistive load in the form of an exponential decay as shown in Figure 20.

Based upon the above captured waveform the calculations regarding energy recapture are calculated as shown below.

The equation governing the regeneration phenomena are given by

$$v(t) = V_0(1-e^{-t/\tau}) \tag{28}$$

where V_0 is the vertical step rise in the waveform and τ is the time constant = RC.

Figure 20 DSO captured waveform during regeneration (see online version for colours)

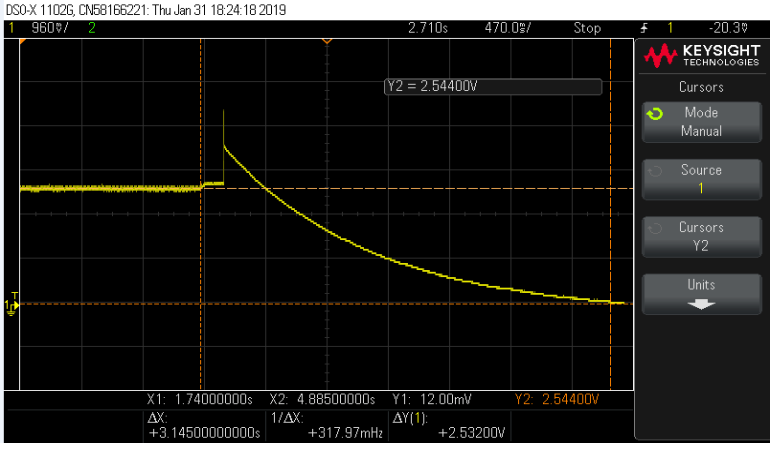

Energy recouping is given by

$$W = \int_{t=0}^{T} \frac{v^2(t)}{R} \mathrm{d}t \tag{29}$$

where T is the time instant at the end of regeneration, corresponding to the DC link voltage reaching initial capacitor voltage

Calculation of W using the captured value V0 and the circuit parameters R yield the result W = 867 J, which corresponds to the stored energy in the drive system only.

10 Conclusion

This paper deals with modelling of an electric automobile covering its mechanical characteristics and calculation of the drive requirements for a typical traffic/road conditions. Further, the requirements on a BLDC motor based drive system are formulated in terms of a typical speed-time characteristic. Two alternate feedback controllers enable the automobile to follow a desired speed trajectory and control the developed shaft torque of the motor. The simulation schematics covering all functional blocks in the problem formulation have been created and a series of simulation runs have been carried out. The set of simulation results corresponding to acceleration and coasting reveal the suitability of the drive system to operate the automobile as dictated by traffic/road conditions. Further, comparison of the overall dynamic performance of the electric vehicle, operating with the above controllers indicates the superiority of the PSO controller

The above work is extended to include the regeneration mode of operation of the drive system during slowing down of the electric vehicle through two alternate schemes, viz., one switch regeneration and auxiliary battery based approach. It has been found that the latter method of regeneration with independent control of the DC-DC converter is capable of higher energy recapture.

To validate the conceptual principles involved in the formulation and simulation, an experimental set up with a representative load has been created. This closed loop configuration consists of a variable voltage variable frequency 6-pulse PWM inverter feeding a 3.7 kW 310 V BLDC machine coupled to a DC generator for loading. This drive system is controlled from an ARM cortex based microcontroller board along with various I/O interfaces for monitoring and control. The experimental results covering the acceleration, coasting and regeneration regions indicate acceptable matching of the speed response and moderate level of energy recapture during regeneration.

Acknowledgements

Authors wish to express their sincere thanks to the Vice Chancellor and Management of SASTRA Deemed University, Thanjavur, India, for extending infrastructural support to carry out the above work in Electric Drives Laboratory.

References

Ananthapadmanabha, B.R., Maurya, R. and Arya, S.R. (2019) 'Hybrid converter for electric vehicle battery charging with power quality features', *International Journal of Computational Systems Engineering*, Vol. 5, No. 1, January, pp.24–35.

Chen, Q., Kang, S., Zeng, L., Xiao, Q., Zhou, C. and Wu, M. (2020) 'PMSM control for electric vehicle based on fuzzy PI', *International Journal of Electric and Hybrid Vehicles*, Vol. 12, No. 1, January, pp.75–85.

Divakarla, K.P., Wirasingha, S.G., Emadi, A. and Razavi, S. (2019) 'Artificial neural network based adaptive control for plug-in hybrid electric vehicles', *International Journal of Electric and Hybrid Vehicles*, Vol. 11, No. 2, January, pp.127–151.

Ehsani, M., Gao, Y., Gay, S.E. and Emadi, A. (2005) *Hybrid Electric, and Fuel Cell Vehicles: Fundamentals, Theory, and Design*, CRC Press LLC, Florida.

Elnaghi, B.E., Ibrahim, H.A., Elsayed, S.A. and Abd-elkader, F. (2020) 'Developed operation of inverter fed induction motor to drive the electric vehicle', *International Journal of Electric and Hybrid Vehicles*, Vol. 12, No. 2, January, pp.116–129.

Godfrey, A.J. and Sankaranarayanan, V. (2018) 'A new electric braking system with energy regeneration for a BLDC motor driven electric vehicle', *Engineering Science and Technology, an International Journal*, Vol. 21, pp.704–713.

Indragandhi, V., Subramaniyaswamy, V., Ravi, L., Vijayakumar, V. and Manimekalai, P. (2020) 'An overview of electric vehicle converter configurations, control methods and charging techniques', *International Journal of Vehicle Information and Communication Systems*, Vol. 5, No. 4, January, pp.406–435.

Khanra, M., Chakraborty, D. and Nandi, A.K. (2018) 'Improvement of regenerative braking energy of fully battery electric vehicle through optimal driving', *Journal of Asian Electric Vehicles*, Vol. 16, No. 1, pp.1789–1798.

Krause, P.C., Wasynczuk, O., Sudhoff, S.D. and Pekarek, S.D. (2013) *Analysis of Electric Machinery and Drive Systems*, Wiley, USA.

Krishnan, R. (2001) *Electric Motor Drives: Modeling, Analysis, and Control*, Prentice Hall, UK.

Li, J., Shu, H., Xu, Z. and Huang, W. (2021) 'Control strategy of genetic algorithm for a hybrid electric container loader', *International Journal of Vehicle Performance*, Vol. 7, Nos. 3–4, January, pp.324–340.

Li, T., Rizzoni, G., Ahmed, Q., Meyer, J., Boesch, M. and Badreddine, B. (2020) 'Model-based electric traction drive resolver fault diagnosis for electrified vehicles', *International Journal of Powertrains*, Vol. 9, Nos. 1–2, January, pp.59–78.

Liu, Z., Lu, S. and Du, R-h. (2020) 'A genetic-fuzzy control method for regenerative braking in electric vehicle', *International Journal of Computing Science and Mathematics*, Vol. 11, No. 3, January, pp.263–277.

MathWorks (2016) *TheMathWorks—MATLAB and Simulink for Technical Computing* [Online], Available: http://www.mathworks.com

Moorthi, V.R. (2005) *Power Electronics: Devices, Circuits, and Industrial Applications*, Oxford University Press, India.

Moussouni, F., Brisset, S. and Brochet, P. (2008) 'Comparison of two multi-agent algorithms: ACO and PSO for the optimization of a brushless DC wheel motor', *Intelligent Computer Techniques in Applied Electromagnetics*, pp.3–10.

Naseri, F., Farjah, E. and Ghanbari, T. (2016) 'An efficient regenerative braking system based on battery/supercapacitor for electric, hybrid, and plug-in hybrid electric vehicles with BLDC motor', *IEEE Transactions on Vehicular Technology*, 20 September, Vol. 66, No. 5, pp.3724–3738.

Nian, X., Peng, F. and Zhang, H. (2014) 'Regenerative braking system of electric vehicle driven by brushless DC motor', *IEEE Transactions on Industrial Electronics*, 14 January, Vol. 61, No. 10, pp.5798–5808.

Proff, H., Szybisty, G. and Fojcik, T.M. (2019) 'From electric cars to energy-efficient houses – the automotive retail sector at the crossroads', *International Journal of Automotive Technology and Management*, Vol. 19, Nos. 1–2, January, pp.55–73.

Pugi, L., Alessandrini, A., Barbieri, R., Berzi, L., Pierini, M., Cignini, F., Genovese, A. and Ortenzi, F. (2021) 'Design and testing of a supercapacitor storage system for the flash recharge of electric buses', *International Journal of Electric and Hybrid Vehicles*, Vol. 13, No. 1, pp.57–80.

Rashid, M.H. (2004) *Power Electronics: Circuits, Devices, and Application*, Pearson Education, India.

Sain, C., Biswas, P.K., Satpathy, P.R., Babu, T.S. and Alhelou, H.H. (2021) 'Self-controlled PMSM drive employed in light electric vehicle-dynamic strategy and performance optimization', *IEEE Access*, Vol. 9, pp.57967–57975, doi: 10.1109/ACCESS.2021.3072910.

Torres-Sanz, V., Sanguesa, J.A., Martinez, F.J., Garrido, P. and Marquez-Barja, J.M. (2018) 'Enhancing the charging process of electric vehicles at residential homes', *IEEE Access*, Vol. 6, 23 April, pp.22875–22888.

Srikanth, R. and Venkatesan, M. (2020) 'Design and modelling of hybrid fuel cell and solar-based electric vehicle', *International Journal of Vehicle Autonomous Systems*, Vol. 15, Nos. 3–4, January, pp.225–240.

Srivastava, M., Verma, A.K. and Tomar, P.S. (2021) 'A comparison of different DC-DC converter topology for electric vehicle charging', *International Journal of Power Electronics*, Vol. 13, No. 1, January, pp.21–44.

Trimboli, M.S., de Souza, A.K. and Xavier, M.A. (2022) 'Stability and control analysis for series-input/Parallel-output cell balancing system for electric vehicle battery packs', *IEEE Control Systems Letters*, Vol. 6, pp.1388–1393, doi: 10.1109/LCSYS.2021.3097875.

Wang, N. and Yang, Q. (2021) 'Optimised design of LCC-S compensation topologies for wireless power transfer with dynamic load for electric vehicles', *International Journal of Vehicle Information and Communication Systems*, Vol. 6, No. 2, January, pp.107–120.

Wu, D., Li, Y., Zhang, J. and Du, C. (2020) 'Optimal regenerative braking torque of permanent-magnet synchronous motor in electric vehicles', *International Journal of Heavy Vehicle Systems*, Vol. 27, No. 3, January, pp.359–386.

Yıldız, B.S. (2020) 'Robust design of electric vehicle components using a new hybrid salp swarm algorithm and radial basis function-based approach', *International Journal of Vehicle Design*, Vol. 83, No. 1, January, pp.38–53.

Zhang, X., Wang, Y., Liu, G. and Yuan, X. (2016) 'Robust regenerative charging control based on T–S fuzzy sliding-mode approach for advanced electric vehicle', *IEEE Transactions on Transportation Electrification*, Vol. 2, No. 1, 25 February, pp.52–65.